PRAMANA
— journal of
physics

Vol. 75, No. 5
November 2010
pp. 947–952

Rate equation simulation of temporal characteristics of a pulsed dye laser oscillator

S KUNDU*, K DASGUPTA, S SASIKUMAR, J SINGH, A K RAY and S SINHA
Laser & Plasma Technology Division, Bhabha Atomic Research Centre,
Mumbai 400 085, India
*Corresponding author. E-mail: skundu@barc.gov.in

Abstract. A time-dependent, two-dimensional (in space) rate equation model of a transversely-pumped pulsed dye laser oscillator, which incorporates transverse pump intensity variation in the presence of intracavity dye laser radiation, is proposed to understand and predict its temporal behaviour. The model yields output pulses which agree well with experimental results using rhodamine 6G and kiton red dyes. The shape, amplitude and temporal position of the simulated pulse within the pump pulse vary dramatically across the tuning range of each dye depending on the relative gain and loss values.

Keywords. Dye laser; numerical model; rate equation; tuning range.

PACS Nos 42.55.Mv; 42.60.Lh; 02.70.Bf

1. Introduction

Wavelength-tunable, narrow-band, high power dye lasers, configured as master-oscillator-power-amplifier (MOPA) systems find widespread applications in many fields such as laser spectroscopy and material processing [1,2]. Among these, copper vapour laser (CVL) pumped dye laser MOPA systems have generated average power up to few kilowatts at a pulse repetition rate of 5–25 kHz and with a pulse duration of a few tens of nanoseconds [3,4]. In MOPA systems, it is essential to have proper temporal synchronization between the pulsed oscillator output and the pulsed gain of the following amplifier to achieve maximum amplification and suppress broadband amplified spontaneous emission (ASE) component. This is a non-trivial problem as the output pulse of the dye oscillator may be significantly smaller than the pump pulse owing to delay in pulse build-up in the cavity. The pulse build-up time and pulse shape depend on various parameters such as cavity losses and wavelength-dependent photophysical constants of the dye, the pump laser parameters, and processes such as gain saturation. Thus, the temporal characteristics of these dye lasers are not uniform across the tuning range of any dye.

To design and build high-power, pulsed dye laser MOPA systems, it is necessary to have a detailed knowledge of the temporal characteristics of the dye laser output, and to understand how sensitively it depends on various dye and pump laser

parameters. Here, an effective model is an invaluable tool, which not only reduces the need for comprehensive time consuming tests, but also helps in qualifying novel design configurations on a virtual test bench. Several authors have used the rate equation-based model to study the performance of dye oscillator [5] and amplifiers [6–10]. In [5], a one-dimensional model with spatially averaged pump intensity at all points was used to describe the evolution of ASE and the dye laser pulse. This ignores an important process, viz., coupled and inter-dependent orthogonal propagation of pump and dye laser inside the gain medium. In this paper, we report the preliminary results of an extended rate equation model for a pulsed dye laser oscillator transversely pumped by the 511-nm component of a CVL, which incorporates coupled propagation of pump and dye laser beam, and compare the computed pulse characteristics with the experimental observations.

2. Rate equation-based model

The model used for simulating the dye laser is based on the time-dependent rate equation description of dye population along with equations describing simultaneous orthogonal propagation of the pump pulse and the evolving intracavity dye laser radiation (see figure 1). Due to short duration of CVL pump pulse, the transfer of population from singlet to triplet state is neglected. It is also assumed that the intensity distributions of both the pump and dye laser, in the direction perpendicular to the plane containing them, are uniform. The coupled rate equations for the system are

$$\frac{\partial N_2(x,y,t)}{\partial t} = N_1(x,y,t)\left[\sigma_{1\mathrm{P}} I_{\mathrm{P}}(x,y,t) + \int \sigma_1^{\lambda} I_{\lambda}^{\pm}(x,y,t)\,\mathrm{d}\lambda\right] - \frac{N_2(x,y,t)}{\tau_2}$$

$$\frac{\partial N_0(x,y,t)}{\partial t} = N_1(x,y,t)\left[\frac{1}{\tau_1} + \sigma_{0\mathrm{P}} I_{\mathrm{P}}(x,y,t) + \int \sigma_{\mathrm{e}}^{\lambda} I_{\lambda}^{\pm}(x,y,t)\,\mathrm{d}\lambda\right] - N_0(x,y,t)\left[\sigma_{0\mathrm{P}} I_{\mathrm{P}}(x,y,t) + \int \sigma_0^{\lambda} I_{\lambda}^{\pm}(x,y,t)\,\mathrm{d}\lambda\right]$$

$$N = N_0 + N_1 + N_2$$

$$\left(\frac{\mu}{c}\frac{\partial}{\partial t} + \frac{\partial}{\partial y}\right) I_{\mathrm{P}}(x,y,t) = -[N_0(x,y,t)\sigma_{0\mathrm{P}} + N_1(x,y,t)\sigma_{1\mathrm{P}}] I_{\mathrm{P}}(x,y,t)$$

$$\left(\frac{\eta}{c}\frac{\partial}{\partial t} \pm \frac{\partial}{\partial x}\right) I_{\lambda}^{\pm}(x,y,t) = [N_1(x,y,t)(\sigma_{\mathrm{e}}^{\lambda} - \sigma_1^{\lambda}) - N_0(x,y,t)\sigma_0^{\lambda}] I_{\lambda}^{\pm}(x,y,t) + \frac{N_1(x,y,t)}{\tau_1} E_{\lambda} F_{\phi}^{\pm}(x).$$

Here, N_0, N_1, N_2 and N are respectively, the ground state, first excited state, second excited state and total population density; $\sigma_{0\mathrm{P}}$ and $\sigma_{1\mathrm{P}}$ are the ground

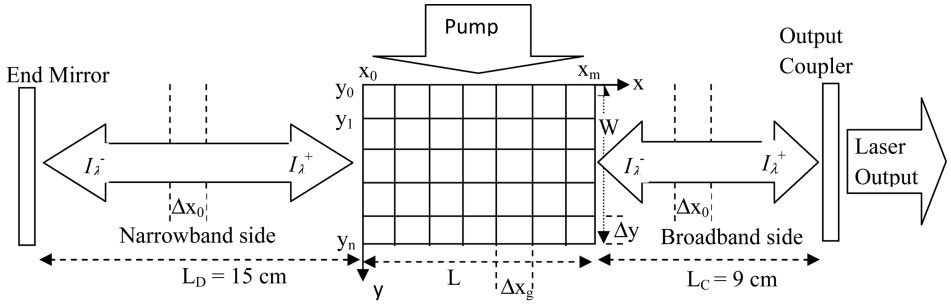

Figure 1. Schematic of transversely pumped dye laser oscillator with two-dimensional space grid.

state absorption (GSA) and excited state absorption (ESA) cross-sections at the pump wavelength; σ_0^λ, σ_1^λ, σ_e^λ are the GSA, ESA, and stimulated emission cross-sections, respectively, at wavelength λ; τ_1 and τ_2 are the lifetimes of the first and second excited states; I_P and $I_\lambda^\pm$ are the pump intensity and dye laser intensity propagating towards $\pm x$ directions at wavelength λ. Also, c is the velocity of light in free space; μ is the refractive index of liquid dye medium (=1.36); E_λ is the spectral contribution at wavelength λ and $F_\phi^\pm$ is the geometrical fraction [8] of fluorescence contributing to the intracavity radiation.

The model geometry for a transversely pumped dye oscillator cavity is shown in figure 1. The gain medium is divided into a two-dimensional square shape space grid (x_i, y_i) with $\Delta x_g = \Delta y = \Delta t c/\mu$. In the free space within the resonator cavity, Δx_0 satisfies the condition $c \cdot \Delta t = \Delta x_0$. The pump pulse duration is divided into time slices of duration Δt, taken as 0.2 ps in the model, to allow reasonable number of grid points along y direction in the gain medium.

The rate equations are converted into centred difference equations where pump and intracavity radiation intensities are calculated during each time interval Δt at the mid-point of each side of the square element, for respective propagation directions and population densities are calculated at the centroid of each square element. The incident $I_P(x_i, y_0)$ is assumed to be constant along the length L of the gain. In ASE components, only on-axis (parallel to the narrow-band laser beam propagation) contributions ($F_\Phi^\pm$) are taken into account. In ASE components, the aspect ratio (L/W) of the gain medium determines the divergence and hence feedback factor. For the narrow-band laser, a time-dependent divergence is calculated on the basis of the second moment of the intracavity intensity distribution along the width W of the gain. The losses at optical components in each arm of the cavity are clubbed into transmission loss of the mirror on that side.

To study the wavelength-dependent temporal characteristics in the model, the fluorescence band of the dye is divided into ten wavelength segments of variable sizes. Smaller size (10 nm) segments are used for wavelength regions within the tuning range and larger size segments are used for the rest of the fluorescence region. This reduces computational time substantially, without masking wavelength-specific pulse characteristics. E_λ is determined from the fluorescence spectrum after the normalization, $\int E_\lambda \, \mathrm{d}\lambda = Q$, where Q is the quantum yield of fluorescence of the dye. τ_2 is taken as 10 ps, representing the rapid non-radiative relaxation to

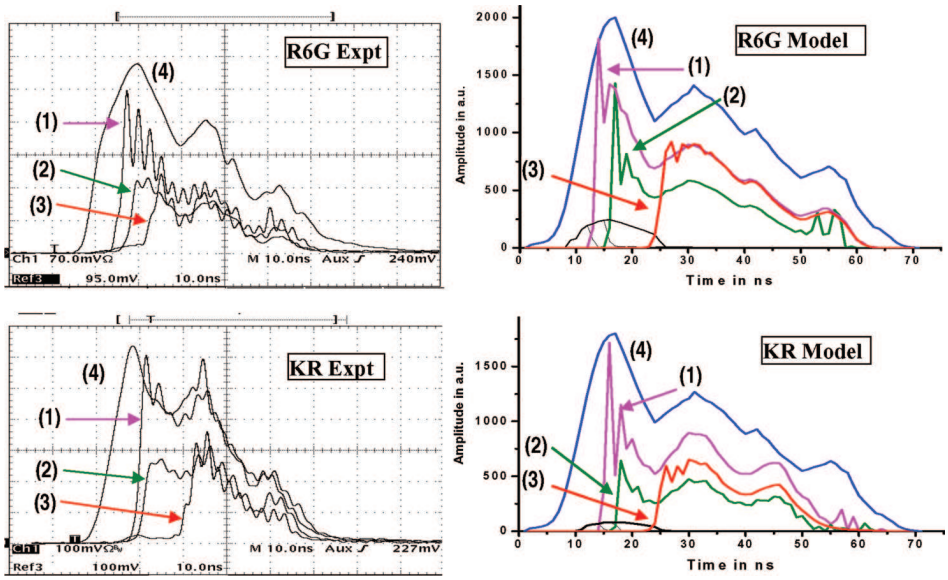

Figure 2. Oscillator output pulse evolution with respect to pump pulse for R6G and KR dyes. Pulse shapes at measured/model wavelengths: (1) at peak of the tuning range; (2) at half-maximum, short wavelength point; (3) at half-maximum, long wavelength point; (4) at pump wavelength. Computed ASE at different wavelengths are shown by traces in black, and appear as pedestals at the start of a recorded pulse.

the first excited state [11]. The molecular cross-sections and other photophysical constants of rhodamine 6G (R6G) are taken from [8] and those of kiton red (KR) are taken from [12].

3. Results and discussion

The output of the model is compared with the experimental results, obtained from separate transversely pumped dye oscillators. The oscillators, pumped by the green component of a CVL-based MOPA chain, are configured in grazing incidence grating configuration, with a 4-prism 25 × beam expander, grating (2400 lines/mm) and output coupler ($R_C = 4\%$). The gain media are ethanolic solution of the dyes (R6G: 0.9 mM, KR: 1.5 mM) with a gain region of dimension 10 mm (L) × 0.3 mm (W) × 0.5 mm (H). Average pump powers of 12 and 9 W are used to pump the R6G and KR oscillators, respectively. Dye laser output powers are measured through an aperture to remove off-axis ASE, and pulse shapes are recorded using a bi-planar photodiode and 500 MHz oscilloscope. The dye laser wavelength is measured using a calibrated wavemeter. Figure 2 compares the model calculations and experimental results of pulse build up delay and pulse shapes for the dyes at different wavelengths.

Table 1.

			λ (nm) (at) half maximum of tuning range					
	Peak λ (nm)		Short λ (nm)		long λ (nm)		Peak efficiency (%)	
Dye	Expt.	Model	Expt.	Model	Expt.	Model	Expt.	Model
R6G	569	573	561	561	584	593	10	14
KR	596	595	588	588	635	614	7	10

The computed results fairly reproduce the experimental pulse characteristics. Some of the differences arise from axial-mode beating modulations, and wavelength-dependent sensitivity of the detector, which are not incorporated in the model. The spectral characteristics are also in good agreement at shorter λ, but show increasing difference as λ increases, as seen in table 1. We find that the results are less sensitive to variations of resonator losses, but depend strongly on photophysical constants of dye and pump pulse shape in the model.

The experimental and model results bring out an interesting observation. The pulses for both dyes at the long-λ half-max point (plots-3), have substantially longer build-up delay than those at short-λ (plots-2), clearly due to smaller σ_e^λ and gain, and yet show same pulse energy efficiency. This is possible only if a significantly higher extraction efficiency compensates for the delayed build-up, despite the smaller σ_e^λ at longer λ and higher saturation intensity. The possible reasons are lower GSA and also a lower diffraction loss brought out by the coupled propagation model. Despite the diffractional divergence being proportional to λ, reduced gain saturation by the dye laser allows the pump to penetrate deeper and produce a wider gain medium, and thus produce a smaller diffractional divergence loss.

4. Conclusions

The results of the two-dimensional coupled propagation model are found to be in qualitative and reasonably good quantitative agreement with experimental results on two separate dye laser oscillators with different dyes. The model is adequate for broadly explaining the influence of different parameters and photophysical processes on the temporal characteristics of the dye laser output.

Acknowledgements

The authors acknowledge C S Rao, J Thomas, S Maurya and J S Dhumal in providing instrumentation and maintenance support during the experiments.

References

[1] V S Letokhov, *Laser photoionization spectroscopy* (Academic, New York, 1987)
[2] L Goldman, in: *Dye laser principles* edited by F J Duarte and L W Hillman (Academic, New York, 1990) Ch. 8
[3] C E Webb, in: *High-power dye lasers* edited by F J Duarte (Springer, Berlin, 1991) Ch. 5
[4] L Bass, R E Bonnano, R P Hackel and P R Hammond, *Appl. Opt.* **31**, 6993 (1992)
[5] L G Nair and K Dasgupta, *IEEE J. Quantum Electron.* **21**, 1782 (1985)
[6] U Ganiel, A Hardy, G Neumann and D Treves, *IEEE J. Quantum Electron.* **11**, 881 (1975)
[7] C C Jensen, in: *High-power dye lasers* edited by F J Duarte (Springer, Berlin, 1991) Ch. 3
[8] A Sugiyama, T Nakayama, M Kato and Y Maruyama, *Appl. Opt.* **36**, 5849 (1997)
[9] K Takehisa, *Appl. Opt.* **36**, 584 (1997)
[10] S V Vasil'ev, M A Kuz'mina and V A Mishin, *Quantum Electron.* **31**, 505 (2001)
[11] R A Hass and M D Rotter, *Phys. Rev.* **A43**, 1573 (1991)
[12] P C Beaumont, D G Jhonson and B J Parsons, *J. Chem. Soc., Faraday Trans.* **94**, 195 (1998)